

Supplemental material is neither peer-reviewed nor thoroughly edited by CJASN. The authors alone are responsible for the accuracy and presentation of the material.

Proteomic analysis of urinary microvesicles and exosomes in medullary sponge kidney disease and autosomal dominant polycystic kidney disease

Maurizio Bruschi^{1*}, Simona Granata^{2*}, Laura Santucci^{1*}, Giovanni Candiano¹, Antonia Fabris², Nadia Antonucci², Andrea Petretto³, Martina Bartolucci³, Genny Del Zotto³, Francesca Antonini³, Gian Marco Ghiggeri⁴, Antonio Lupo², Giovanni Gambaro², Gianluigi Zaza²

¹ Laboratory on Molecular Nephrology, IRCCS Istituto Giannina Gaslini, Genoa, Italy.

² Renal Unit, Department of Medicine, University-Hospital of Verona, Italy

³ Core Facilities, IRCCS Istituto Giannina Gaslini, Genoa, Italy.

⁴ Division of Nephrology, Dialysis and Transplantation, IRCCS Istituto Giannina Gaslini, Genoa, Italy.

Supplemental material is neither peer-reviewed nor thoroughly edited by CJASN. The authors alone are responsible for the accuracy and presentation of the material.

Table of contents for supplemental materials

Supplemental methods

Supplemental Figure 1. Age and eGFR of all study participants included in the study.

Supplemental Figure 2. Characterization of isolated exosomes and microvesicles

Supplemental Figure 3. Gene Ontology annotation of urinary extracellular vesicle proteins.

Supplemental Figure 4. Multidimensional scaling analysis of extracellular vesicles from the urine of medullary sponge kidney (MSK) and autosomal dominant polycystic kidney disease (ADPKD) patients.

Supplemental Figure 5. Sample clustering and trait indicators.

Supplemental Figure 6. Venn diagram of statistically significant differences in protein abundance in the different types of extracellular vesicles from medullary sponge kidney (MSK) or autosomal dominant polycystic kidney disease (ADPKD) patients.

Supplemental Figure 7. Proteins network interaction.

Supplemental Figure 8. Gene Ontology enrichment analysis for core discriminatory proteins in the extracellular vesicles of medullary sponge kidney (MSK) and autosomal dominant polycystic kidney disease (ADPKD) patients.

Supplemental Table 1. List of all significant proteins identified using mass spectrometry

Supplemental Table 2. ELISA cutoff, sensitivity, specificity and likelihood ratio.

References for supplemental materials

Supplemental methods

Mass spectrometry: Instrumentation

The desalted peptides were dried by speed vacuum and resuspended in 2% acetonitrile containing 0.2% formic acid (FA). They were separated on a 50-cm reversed-phase Easy Spray column (75- μ m internal diameter \times 50 cm; 2 μ m/100 Å C18) on an Ultimate 3000 RSLCnano system (Thermo Fisher Scientific, Waltham, MA, USA) with a binary buffer system comprising buffer A (0.1% FA) and buffer B (80% acetonitrile, 5% dimethylsulfoxide, 0.1% FA). The program comprised a 70-min gradient (2–45% buffer B) at a flow rate of 250 nl per min, with the column temperature maintained at 60°C. The chromatography system was coupled to an Orbitrap Fusion Tribrid mass spectrometer (Thermo Fisher Scientific), acquiring data in Charge Ordered Parallel Ion aNalysis (CHOPIN) mode [1]. The precursors were ionized using an EASY-spray source held at +2.2 kV and the inlet capillary temperature was held at 300°C. Single MS survey scans were performed over the mass window 375–1500 m/z with an AGC target of 250,000, a maximum injection time of 50 ms, and a resolution of 120,000 at 200 m/z . Monoisotopic precursor selection was enabled for peptide isotopic distributions, precursors of $z = 2-5$ were selected for 2 s of cycle time, and dynamic exclusion was set to 25 s with a ± 10 ppm window set around the precursor. The following CHOPIN conditions were applied: a) if the precursor charge state is 2, then follow with collision-induced dissociation (CID) and scan in the ion trap with an isolation window of 1.8, CID energy of 35% and a rapid ion trap scan rate; b) if the precursor charge state is 3–5 and precursor intensity $>500,000$, then follow with higher-energy C-trap dissociation (HCD) and scan in the Orbitrap with an isolation window of 1.8, HCD energy of 28% and a resolution of 15000; c) if the precursor charge state is 3–5 and precursor intensity $<500,000$, then follow with CID as described for option

Supplemental material is neither peer-reviewed nor thoroughly edited by CJASN. The authors alone are responsible for the accuracy and presentation of the material.

(a). For all MS² events, the following options were set: “Injection Ions for All Available Parallelizable Time” with an AGC target value of 4000 and a maximum injection time of 250 ms for CID, or an AGC target value of 10,000 and a maximum injection time of 40 ms for HCD.

Mass spectrometry: Data analysis

Raw MS files were processed within the MaxQuant v1.6.0.16environment [2] using the MaxLFQ algorithm for label-free quantification and the integrated Andromeda search engine with a false discovery rate (FDR) <0.01 at the protein and peptide levels. The search included variable modifications for oxidized methionine (M), acetylation (protein N-terminus), and fixed carbamidomethyl modifications (C). Up to two missed cleavages were allowed for protease digestion. Peptides with at least six amino acids were considered for identification, and ‘match between runs’ was enabled with a matching time window of 1 min to allow the quantification of MS¹ features which were not identified in each individual measurement. Peptides and proteins were identified using the UniProt FASTA *Homo sapiens* database (August 2017).

Dynamic light scattering

The size of the exosomes and microvesicles were determined by dynamic light scattering (DLS) using a Zetasizer nano ZS90 particle sizer at a 90° fixed angle (Malvern Instruments, Worcestershire, UK). The particle diameter was calculated using the Stokes–Einstein equation [3]. For particle sizing in solution, exosome or microvesicle aliquots were diluted in 10% PBS and analyzed at a constant 25°C. The data were acquired and analyzed using Dispersion Technology Software (Malvern Instruments).

Supplemental material is neither peer-reviewed nor thoroughly edited by CJASN. The authors alone are responsible for the accuracy and presentation of the material.

Western blot

The protein content of microvesicles and exosomes was measured by Bicinchoninic acid assay. Samples (5 µg total protein for all type of extracellular vesicles) were separated by sodium dodecylsulfate polyacrylamide gel electrophoresis (SDS-PAGE) on an 8–16% acrylamide gradient and then transferred to a nitrocellulose membrane. The membrane was blocked, rinsed and labeled with one of the following primary human antibodies diluted in 1% (w/v) bovine serum albumin (BSA) in PBS containing 0.15% (v/v) Tween-20 (PBS-T): monoclonal anti-CD63 (Novus Biological, Littleton, CA, USA, 1:1000 clone H5C6), monoclonal anti-CD81 (Novus Biological, 1:1000 clone 1D6), or monoclonal anti-CD45 (LifeSpan BioSciences, Seattle, WA, USA, 1:1000 clone 3G4). After rinsing in PBS-T, the membrane was probed with secondary antibodies conjugated to horseradish peroxidase (diluted 1:10,000 in 1% (w/v) BSA in PBS-T). Chemiluminescence was monitored using the ChemiDoc Touch Imaging System (Bio-Rad, Hercules, CA, USA) and the signal was quantified by densitometry using Image Lab software (Bio-Rad).

Flow cytometry: Instrumentation

Before exosomes acquisition, the LSRFortessa X-20 instrument (Becton Dickinson Franklin Lakes, NJ, USA) was calibrated using CS&T beads (Becton Dickinson) and carefully washed with double-distilled water for at least 1 h. Front scatter (FSC) and side scatter (SSC) were set to log scale as recommended [4], and voltages were adjusted to the highest values to exclude background noise from PBS [4], which was purified by passing through 0.22-µm UltrafreeVR-MC/DuraporeVR-PVDF centrifugal filter units (Merk, Darmstadt, Germany). This allowed the detection of all different dimensions (0.5, 0.24, 0.2, 0.16 µm) of SSC MegaMix beads (BioCytex, Stago Group, France). For every sample

Supplemental material is neither peer-reviewed nor thoroughly edited by CJASN. The authors alone are responsible for the accuracy and presentation of the material.

acquisition, Rainbow Fluorescent Particles (Spherotech, Lake Forest, IL, USA) were used to adjust all channel voltages thus maintaining voltage consistency. Monoclonal mouse anti-human CD63 (IgG1, clone H5C6), CD81 (IgG1, clone JS-81) and IgG1 isotype controls (clone MOPC-21) were sourced from Becton Dickinson whereas CD133PE-Cy7 (IgG1, clone7) was sourced from BioLegend (San Diego, CA, USA). FITC-conjugated phalloidin was provided by Sigma-Aldrich (St. Louis, MO, USA).

Flow cytometry: Analysis

Exosomes, identified as particles smaller than 0.16 μm in diameter when compared to SSC MegaMix Beads, were gated according to their SSC, and 100,000 events for each sample were acquired at a low sample pressure and a low flow rate of 8–12 $\mu\text{l}/\text{min}$ [4]. Fluorescence Minus One (FMO) analysis was used to achieve the correct size cutoff [5]. FCS files were exported from Fortessa X20 and data were evaluated using Kaluza software (Beckman Coulter, Brea, CA, USA).

CD133 ELISA assay

CD133 expression in urinary exosomes was determined by homemade ELISA. Clean exosome fraction recovered from 16 ml of urine was solubilized in 10 μl of mild detergent solution i.e. 1%(v/v) Nonident P-40 (NP-40), 0.5%(v/v) Tween-20 in PBS and stored at -80°C until use. 96-well maxi-sorp-nunc-immuno plates (ThermoFisher Scientific, MA, USA) were coated overnight at 4°C with Anti-CD133 antibody (United States Biological, USA) diluted 1:10 in PBS. After blocking with 3%(w/v) Bovine serum Albumin (BSA) in PBS, 100 μl of diluted sample (1:10) were added per well and incubated overnight at 4°C. Samples were, then, washed five times with PBS and 0.15%(v/v) Tween-20 (PBS-T) and incubated

Supplemental material is neither peer-reviewed nor thoroughly edited by CJASN. The authors alone are responsible for the accuracy and presentation of the material.

4 hours with anti-CD133 mouse monoclonal antibody (United States Biological, USA, clone 2F8C5) diluted 1:1000 with 1%BSA(w/v) in PBS-T. After three washes with PBS-T, conjugated HRP anti-mouse IgG diluted 1:5000 were added and incubated 1 hour. Samples were washed again three times with PBS-T and one time with PBS before adding the peroxidase substrate (TMB, Bio-Rad). The reaction was stopped with a H₂SO₄ solution. Absorbance at 450 nm was measured using Mark microplate Absorbance Spectrophotometer (Bio-Rad). To standardize the response of the antibodies, a pool of highly positive control was used. The optical density results were expressed as Relative Unit per ml (RU/ml).

Statistical analysis

After normalization, mass spectrometry data were analyzed by unsupervised hierarchical clustering using multidimensional scaling (MDS) with k-means and Spearman's correlation to identify outliers and the dissimilarity between samples. The normalized expression profiles of the proteins were then used to construct the co-expression network using the weighted gene co-expression network analysis (WGCNA) package in R [6]. A weighted adjacency matrix was constructed using the power function. After choosing the appropriate β parameter of power (with the value of independence scale set to 0.8) the adjacency matrix was transformed into a topological overlap matrix (TOM), which measures the network connectivity of all the proteins. To classify proteins with co-expression profiles into protein modules, hierarchical clustering analysis was conducted according to the TOM dissimilarity with a minimum size of 30 proteins per module. To identify the relationship between each module and clinical trait, we used module eigengenes (MEs) and calculated the correlation between MEs and each clinical trait and their statistical significance

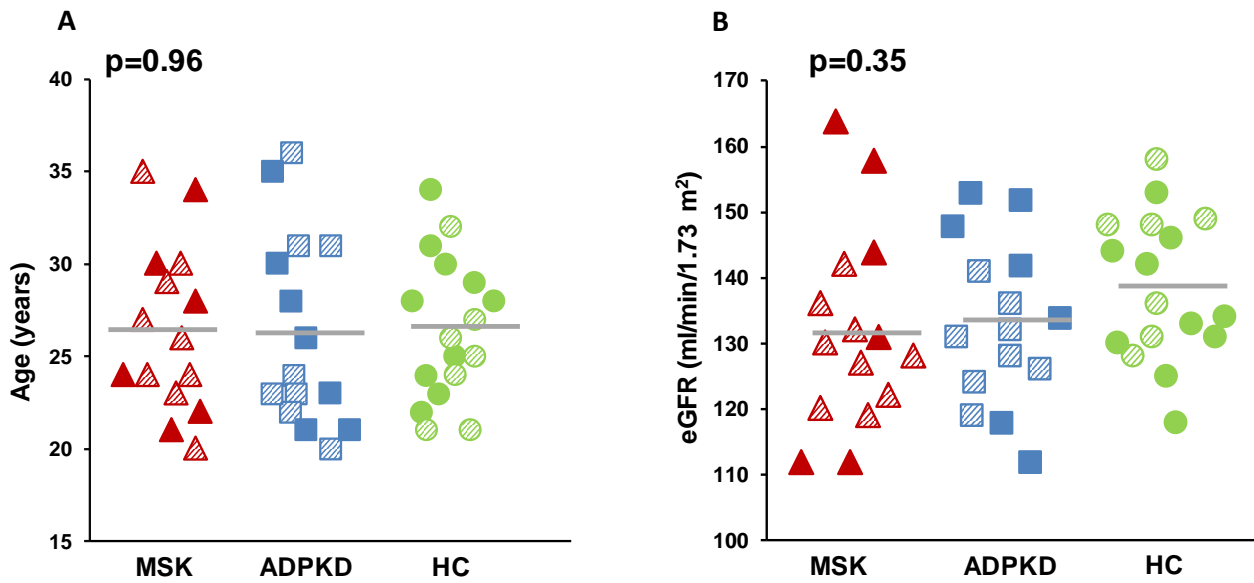
Supplemental material is neither peer-reviewed nor thoroughly edited by CJASN. The authors alone are responsible for the accuracy and presentation of the material.

corrected for multiple interactions. A heat map was then used to visualize the degree and significance of each relationship.

To identify the hub proteins of modules that maximize the discrimination between the selected clinical traits, we applied a non-parametric Mann–Whitney U test, machine learning methods such as non-linear support vector machine (SVM) learning, and partial least squares discriminant analysis (PLS-DA). For the Mann–Whitney U test, proteins were considered to be significantly differentially expressed between the two conditions with power of 80% and an adjusted P-value ≤ 0.05 after correction for multiple interactions (Benjamini-Hochberg) and a fold change of ≥ 2 . In addition, the proteins needed to show at least 70% identity in the samples in one of two conditions. Volcano plots were used to visualize this analysis. In SVM learning, a fourfold cross-validation approach was applied to estimate the prediction and classification accuracy. Besides, the whole matrix was randomly divided into two part. One for learning (65%) and the other one (35%) to verify the accuracy of the prediction. Finally, the resulting core panel of hub proteins was uploaded to Cytoscape to construct a protein–protein interaction network and identify the principal biological processes and pathways involved in the modules corresponding to each clinical trait. Gene Ontology (GO) annotations were extracted from the UniProt, Reactome, KEGG and ClueGO databases and presented on a heat map and two-dimensional scatter plot.

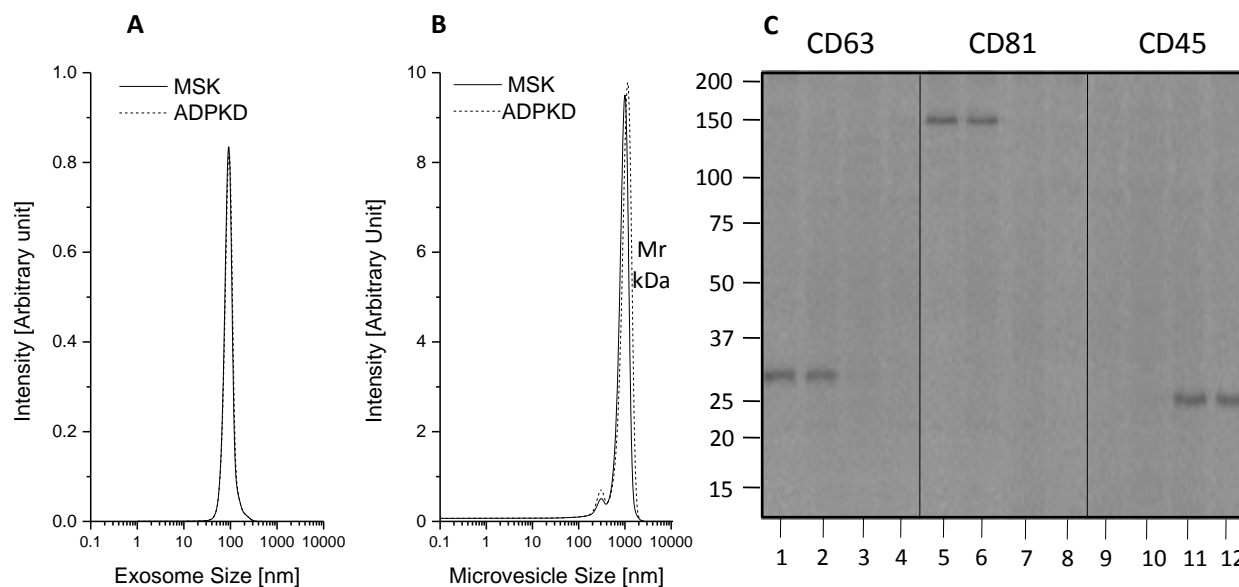
For ELISA data analysis, the Kruskal-Wallis test was used to assess differences in CD133 protein levels among the three study groups, and the results were expressed as medians and IQ ranges. A value of $P < 0.05$ was considered to be statistically significant. Received operating characteristic (ROC) curves were generated to assess the diagnostic efficiency of each assay. Youden's index was used to identify the cutoff [7]. All statistical tests were performed using the latest version of software package *R* available at the time of the experiments.

Supplemental Figure 1. Age and eGFR of the study participants.



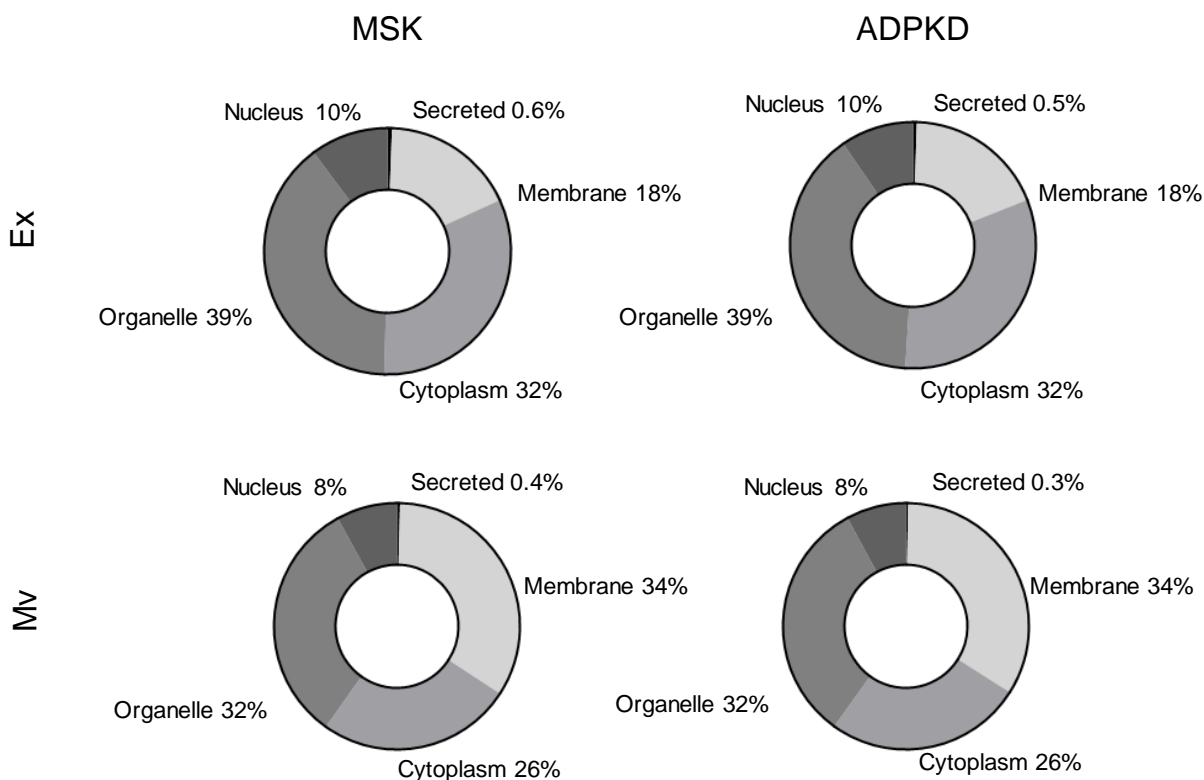
Dot plots represent (A) age and (B) eGFR measured by CKD-EPI Equations of all study participants. Full triangles, squares and circles indicate male subjects while triangles, squares and circles with diagonal stripes indicate female patients. The line represents the mean value.

Supplemental Figure 2. Characterization of isolated exosomes and microvesicles.



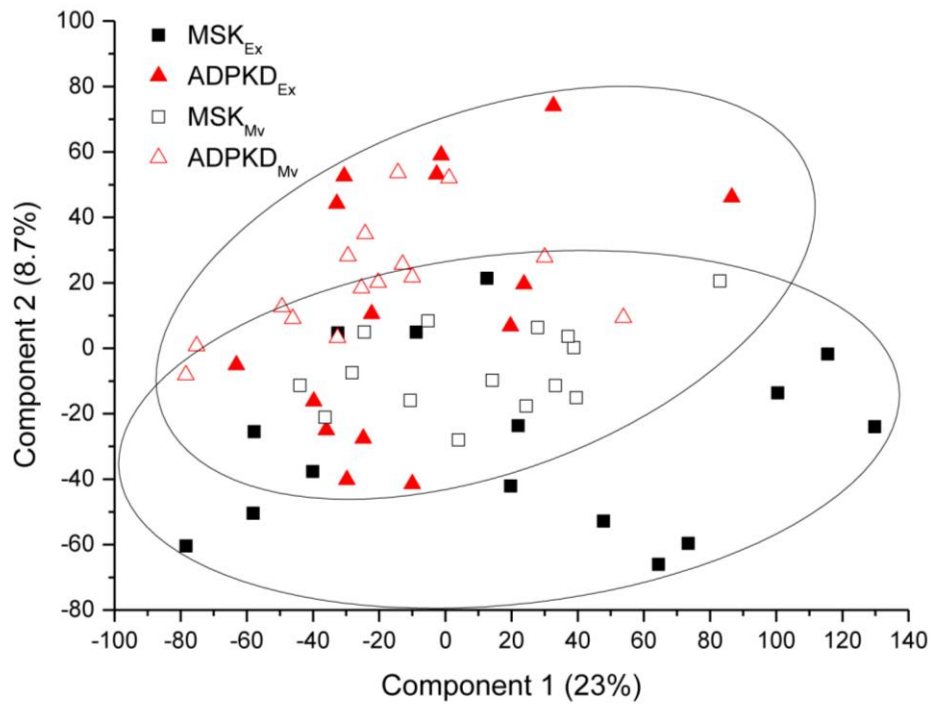
Plot of exosomes **(A)** and microvesicles **(B)** size distribution, as evaluated by dynamic light scattering. The plot shows a Gaussian distribution profile with a mean peak at 90 ± 5 nm or 1000 ± 70 nm respectively for exosomes or microvesicles. No statistical differences were observed between the exosomes or microvesicles isolated from the urine of medullary sponge kidney (MSK) and autosomal dominant polycystic kidney disease (ADPKD) patients. **(C)** Representative western blot analysis of exosomes and microvesicles isolated from the urine of medullary sponge kidney (MSK) and autosomal dominant polycystic kidney disease (ADPKD) patients. Whole exosomes (lanes 1–2, 5–6 and 9–10) and microvesicles (lanes 3–4, 7–8 and 11–12) from MSK (lanes 1, 3, 5, 7, 9 and 11) and ADPKD (lanes 2, 4, 6, 8, 10 and 12) patients were analyzed by detecting CD63 (lanes 1–4), CD81 (lanes 5–8) and CD45 (lanes 9–12). Stain-free technology was used as loading control.

Supplemental Figure 3. Gene Ontology annotation of urinary extracellular vesicle proteins.



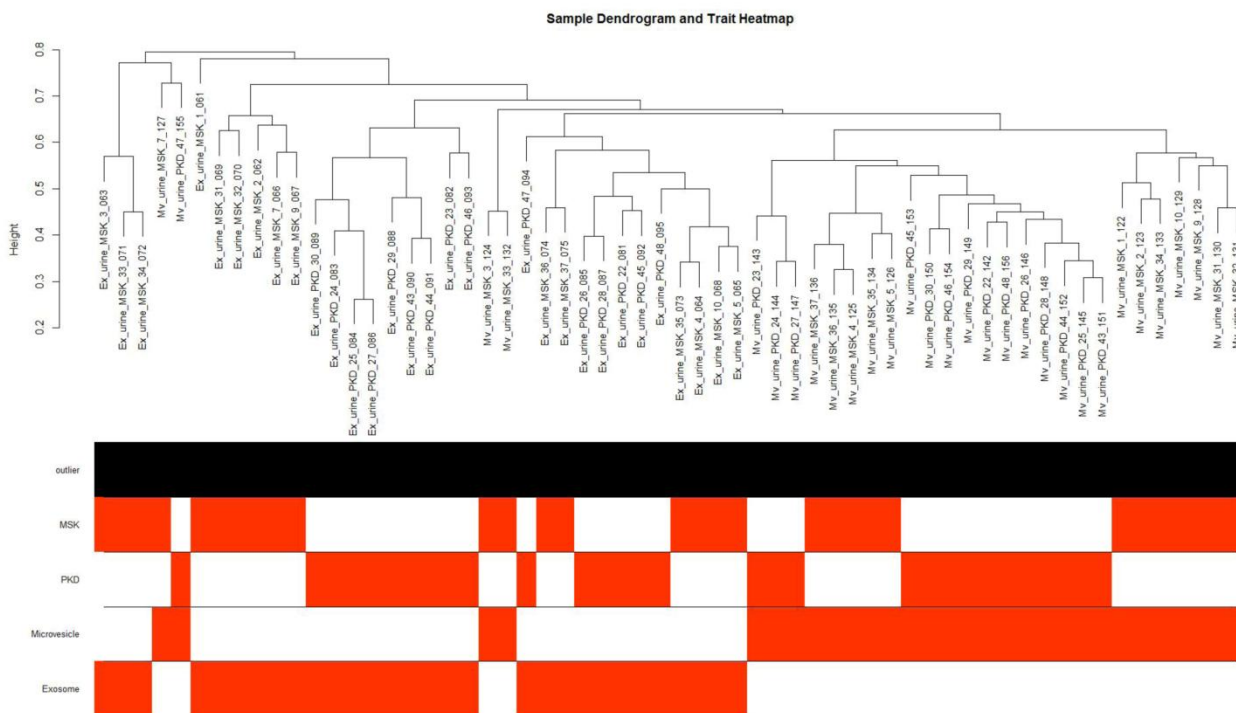
The pie charts show the distribution of cellular component annotations in the different conditions. The percentage distribution of cellular component categories is similar between the exosomes of medullary sponge kidney (MSK) and autosomal dominant polycystic kidney disease (ADPKD) patients, and between the microvesicles of medullary sponge kidney (MSK) and autosomal dominant polycystic kidney disease (ADPKD) patients.

Supplemental Figure 4. Multidimensional scaling analysis of extracellular vesicles from the urine of medullary sponge kidney (MSK) and autosomal dominant polycystic kidney disease (ADPKD) patients.



Two-dimensional scatter plot of MDS analysis of exosomes (solid symbol) and microvesicles (open symbol) of medullary sponge kidney (MSK) (red triangle) and autosomal dominant polycystic kidney disease (ADPKD) (black square) samples. Ellipsis indicates 95% confidence interval. No outliers were detected.

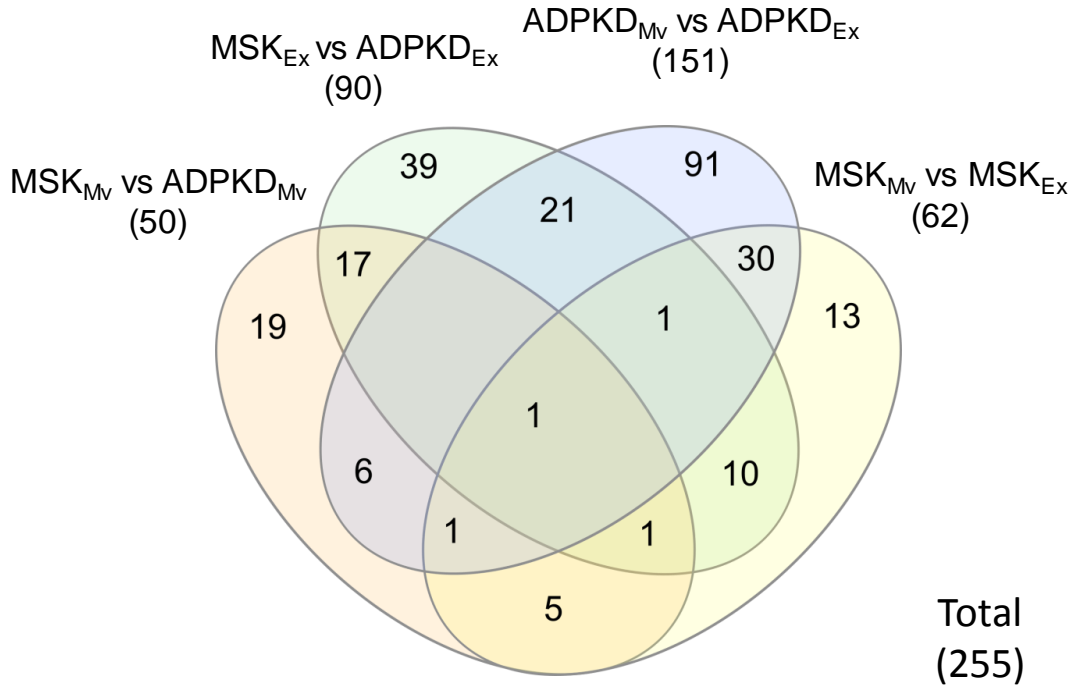
Supplemental Figure 5. Sample clustering and trait indicators.



In the upper panel, the clustering of samples was based on the label-free quantification of proteins identified by mass spectrometry. In the lower panel, the color intensity was proportional to the trait indicator classification, i.e. the type of pathology and extracellular vesicle. No outliers were detected.

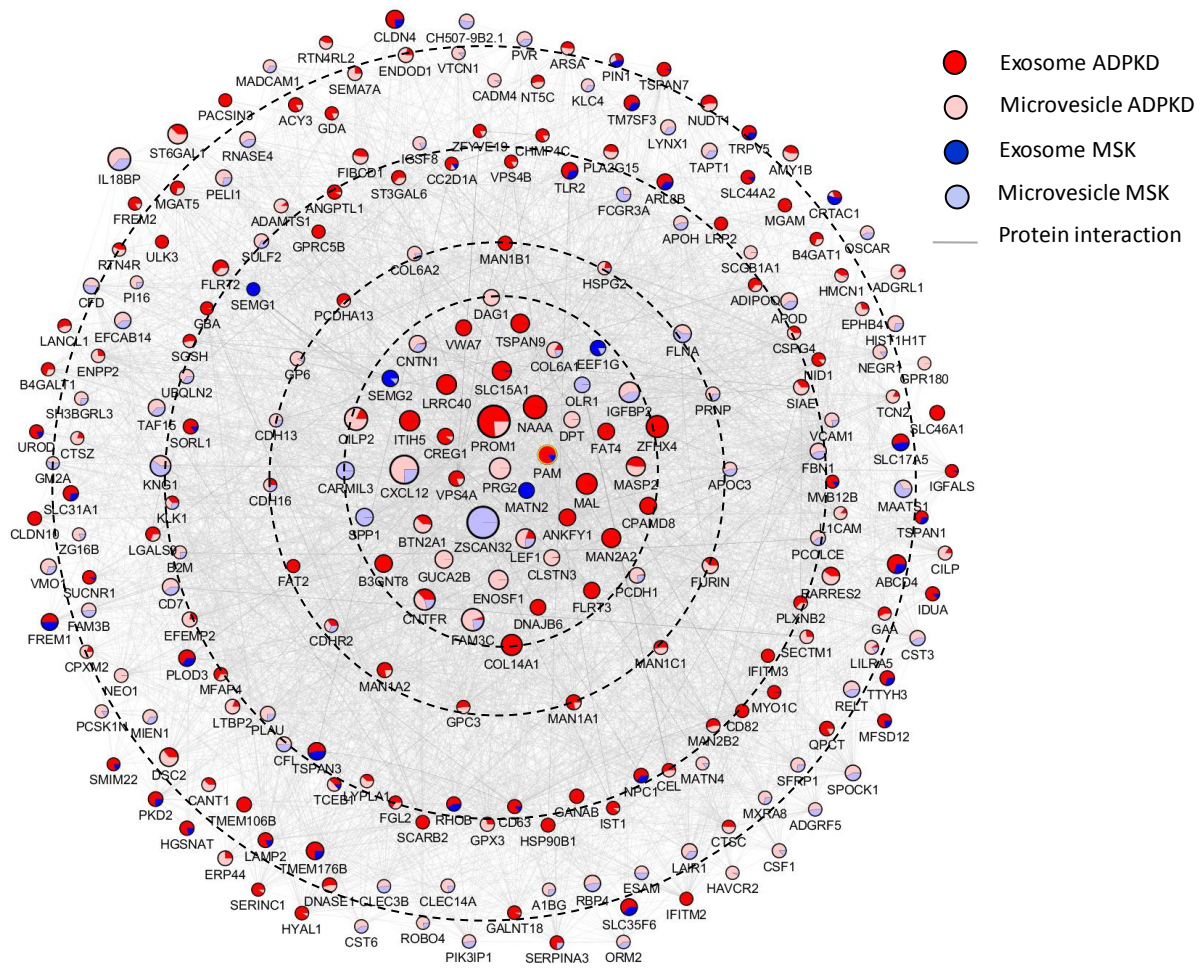
Supplemental material is neither peer-reviewed nor thoroughly edited by CJASN. The authors alone are responsible for the accuracy and presentation of the material.

Supplemental Figure 6. Venn diagram of statistically significant differences in protein abundance in the different types of extracellular vesicles from medullary sponge kidney (MSK) or autosomal dominant polycystic kidney disease (ADPKD) patients.



Venn diagram shows common and exclusive peptides. The numbers represent the distinct proteins in the overlapping and non-overlapping areas.

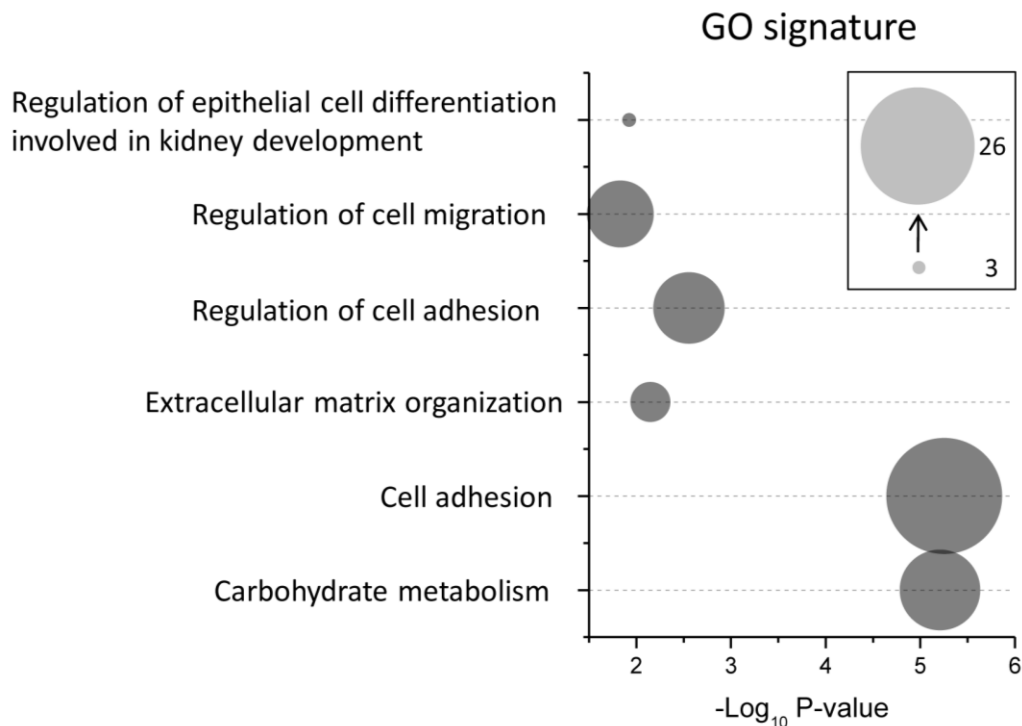
Supplemental Figure 7. Network of proteins interaction.



Network of proteins interaction. The diagram report all the interaction between the 255 statistically significant proteins. Circles and grey lines correspond respectively, to proteins and their interactions. Circles size and colours are related respectively, to the number of protein interactions and the relative expression, after Z-score, in the four conditions i.e. ADPKD exosomes (dark red) and microvesicles (light red), and MSK exosome (dark blue) and microvesicles (light blue). Besides, the proteins are grouped into four classes (dotted ellipses) in function of the type of protein interaction and their ability to distinguish the four conditions. These classes correspond from outside to inside, respectively, to proteins: 1) linked by only co-expression and co-localization interactions, 2) with also physical interactions, 3) also linked by biochemical pathway and 4) that maximize the discrimination between the four conditions.

Supplemental material is neither peer-reviewed nor thoroughly edited by CJASN. The authors alone are responsible for the accuracy and presentation of the material.

Supplemental Figure 8. Gene Ontology enrichment analysis for core discriminatory proteins in the extracellular vesicles of medullary sponge kidney (MSK) and autosomal dominant polycystic kidney disease (ADPKD) patients.



The $-\log_{10}$ (P value) of each term is shown on the x-axis and the enriched GO terms are shown on the y-axis. The size of each circle is proportional to the number of proteins associated with each GO term.

Supplemental material is neither peer-reviewed nor thoroughly edited by CJASN. The authors alone are responsible for the accuracy and presentation of the material.

Supplemental Table 1. List of all significant proteins identified using mass spectrometry. The symbol “+” identify the significant proteins in each experimental comparison. Fold change value is reported as mean and standard deviation.

Uniprot ID	Protein name	Gene name	Significant ADPDK-Mv vs MSK-Mv	Significant ADPDK-Ex vs MSK-Ex	Significant ADPDK-Ex vs ADPDK-Mv	Significant MSK-Ex vs MSK-Mv	Fold Change ADPDK-Mv vs MSK-Mv	P-value ADPDK-Mv vs MSK-Mv	Fold Change ADPDK-Ex vs MSK-Ex	P-value ADPDK-Ex vs MSK-Ex	Fold Change ADPDK-Ex vs ADPDK-Mv	P-value ADPDK-Ex vs ADPDK-Mv	Fold Change MSK-Ex vs MSK-Mv	P-value MSK-Ex vs MSK-Mv
A0A075B7C1	Cyclic AMP-dependent transcription factor ATF-1	FUS			+		1.72±3.91		0.09±1.27		-7.29±4.17	10.31	-5.65±4.51	
A0A087WTQ1	Solute carrier family 15 member 1	hPEPT1-RF		+	+		-1.11±1.68		1.96±1.95	2.42	3.57±2.21	7.62	0.5±1.96	
A0A087WU36	Plexin-B2	PLXNB2		+			2.12±2.84		3.13±2.56	3.63	0.68±1.72		-0.33±2.88	
A0A087WU85	Major facilitator superfamily domain-containing protein 12	MFSD12			+		-0.47±1.15		1.25±2.95		3.21±2.51	4	1.5±2.55	
A0A087WV23	SH3 domain-binding glutamic acid-rich-like protein 3	SH3BGRL3			+		0.91±1.81		0.66±2.24		-2.05±1.77	3.22	-1.8±2.66	
A0A087WV34	Glycosylated lysosomal membrane protein	GLMP			+		-1.34±1.66		0.66±2.16		4.72±2.96	7.23	2.72±2.39	
A0A087WWC0	Mucosal addressin cell adhesion molecule 1	MADCAM1			+		0.92±3		-0.07±2.79		-3.32±3.5	2.16	-2.32±2.91	
A0A087WWY3	Filamin-A	FLNA			+	+	-0.84±1.62		0.38±2.19		-3.73±2.78	4.48	-4.94±3.05	7.66
A0A087WXB8	Type 2 lactosamine alpha-2,3-sialyltransferase	ST3GAL6		+			1.77±2.11		3.99±2.91	4.73	0.77±2.23		-1.45±1.9	
A0A087WY93	Alpha-1-antichymotrypsin	SERPINA3		+			-0.33±1.21		1.27±1.07	3.43	0.73±1.02		-0.87±1.2	
A0A087WY93	Alpha-1-antichymotrypsin	SERPINA3		+			-0.33±1.21		1.27±1.07	3.43	0.73±1.02		-0.87±1.2	
A0A087WYG6		LYNX1			+		1.72±4.11		-0.12±2.6		-6.28±4.06	6.57	-4.43±4.63	

Supplemental material is neither peer-reviewed nor thoroughly edited by CJASN. The authors alone are responsible for the accuracy and presentation of the material.

A0A087WZ31	Mannosyl-oligosaccharide 1,2-alpha-mannosidase IC	MAN1C1						4.36±2.63		4.51±3.48	4.11	0.27±2.08		0.13±2.09	
A0A087WZG7	Cadherin-13	CDH13						1.8±3.42		2.37±3.3		-3.54±3.35	2.67	-4.11±4.11	
A0A087X064	Endoplasmic reticulum mannosyl-oligosaccharide 1,2-alpha-mannosidase	MAN1B1						-0.41±1.41		3.59±3.66		4.78±3.53	4.6	0.79±2.37	
A0A087X0I2	Complement factor I	CFI						0.02±1.17		-0.04±1.32		-1.65±1.7	2.24	-1.59±1.23	4.09
A0A087X0S5	Collagen alpha-1	COL6A1						0.63±1.45		1.71±1.68	2.46	-0.7±1.5		-1.78±1.65	2.78
A0A087X137	Leukocyte-associated immunoglobulin-like receptor 1	LAIR1						1.23±2.21		-1.46±2.37		-5.44±3.36	7.67	-2.74±2.84	
A0A087X1J7	Glutathione peroxidase 3	GPX3						4.62±3.43	4.7	3.53±3.67		-1.73±2.9		-0.64±2.94	
A0A087X1K9	Acyl-protein thioesterase 1	LYPLA1						5.73±3.2		1.54±2.71		-0.86±1.41		3.33±3.06	2.83
A0A087X1L8	ICOS ligand	ICOSLG						-0.22±2.14		-0.09±2.19		-2.81±2.54	2.92	-2.94±2.65	2.93
A0A087X1M4	V-set domain-containing T-cell activation inhibitor 1	VTCN1						2±2.51		0.24±2.77		-3.48±3.07	3.07	-1.73±2.77	
A0A096LP62	Inter-alpha-trypsin inhibitor heavy chain H5	ITIH5						-0.38±1.61		4±2.92	4.72	4.22±2.7	6.8	-0.16±2.06	
A0A0A0MQT7	Collagen alpha-1	COL14A1						-1.15±1.93		4.61±3.08	5.99	4.87±3.17	6.48	-0.89±1.89	
A0A0A0MQX7	Testican-1	SPOCK1						0.45±1.94		1.19±2		-2.69±2.53	2.7	-3.43±2.43	5.1
A0A0A0MRS3	Basement membrane-specific heparan sulfate proteoglycan core protein	HSPG2						1.03±1.79		2±1.77	3.03	-0.81±1.61		-1.77±1.83	
A0A0A0MSA9	Poliovirus receptor	PVR						0.48±1.57		0.57±2.25		-2.52±2.1	3.47	-2.62±2.51	2.58
A0A0A0MSK1	Angiopoietin-related protein 1	ANGPTL1						1.21±2.47		3.55±2.57	4.84	2.01±2.69		-0.33±1.73	
A0A0A6YY98	Transient receptor potential cation channel subfamily V member 6	TRPV6						0.06±1.53		1.32±3.41		4.62±3.25	5.19	3.36±3.37	
A0A0B4J288	Cadherin-16	CDH16						0.31±1.56		2.44±2.72		-0.33±2.08		-2.45±2.34	2.63
A0A0C4DFP6	Cartilage acidic protein 1	CRTAC1						3.25±2.54		-0.72±2.72		0.46±1.99		4.42±3.46	4.01
A0A0C4DFZ2	Arylsulfatase A	ARSA						1.97±2.18		2.52±2.46	2.49	-0.12±1.73		-0.67±2.28	
A0A0C4DGG1	Protein kinase C and casein kinase substrate in neurons protein 3	PACSIN3						1±1.94		2.06±2.87		1.85±1.88	2.31	0.79±2.83	
A0A0C4DGL1	Alpha-mannosidase 2x	MAN2A2						0.05±1.84		3.88±2.98	4.17	4.62±3.17	5.58	0.79±1.99	
A0A0C4DGN4	Zymogen granule protein 16 homolog B	ZG16B						1.23±2.97		0.5±2.25		-2.25±2.31	2.28	-1.53±3.15	
A0A0C4DGV7	Retinol-binding protein 4	RBP4						0.25±1.32		0.38±1.66		-2.58±2.2	3.27	-2.7±1.81	5.91

Supplemental material is neither peer-reviewed nor thoroughly edited by CJASN. The authors alone are responsible for the accuracy and presentation of the material.

A0AV65	Neural cell adhesion molecule L1	L1CAM	+					2.11±2.23	2.21	1.57±2.5		-1.35±2.45		-0.82±1.97
A0AV84	Leucine-rich repeat transmembrane protein FLRT2	FLRT2	+	+				4.01±3.26	3.78	3.73±2.94	3.92	0.95±2.11		1.23±2.72
A0AVK2	Cilia- and flagella-associated protein 91	MAATS1			+	+		-1.56±2.27		0.74±2.36		-3.45±3.05	3.06	-5.76±3.51 8.02
A1L3U4	Cadherin-related family member 2	CDHR2		+				0.06±2.36		2.53±2.23	3.07	0.01±1.66		-2.46±2.77
A2A2V1	Major prion protein	PRNP			+			1.05±1.76		0.89±2.4		-2.5±1.86	4.49	-2.35±2.8
A2A2Z9	Ankyrin repeat domain-containing protein 18B	ANKRD18B		+	+			1.12±1.69		5.43±3.91	4.89	4.81±3.71	4.15	0.5±1.56
A2BEX8	von Willebrand factor A domain-containing protein 7	VWA7		+	+			0.69±2.25		2.86±2.56	2.98	2.83±2.82	2.39	0.66±1.9
A2N6W9	Low affinity immunoglobulin gamma Fc region receptor III-A	FCGR3A				+		-1.46±2.13		-0.11±2.3		-2.34±2.64		-3.7±2.67 4.85
A3KFJ8	Fibrinogen C domain-containing protein 1	FIBCD1	+	+				3.38±2.67	4.06	3.73±3.35	2.96	-0.25±2.55		-0.61±2.27
A4D108	Transmembrane protein 106B	TMEM106B			+			0.5±1.66		2.97±3.07		3.62±2.44	5.81	1.15±2.77
A4D201	Protein tweety homolog 3	TTYH3			+			-1.64±2.36		1.51±2.16		5.16±3.55	5.5	2.01±2.31
A4D205	7,8-dihydro-8-oxoguanine triphosphatase	NUDT1	+	+				3.18±2.62	3.67	4.48±3.16	5.19	0.3±1.34		-1±2.7
A4D232	DnaJ homolog subfamily B member 6	DNAJB6		+	+			0.07±2.46		2.65±2.5	2.67	2.05±2.05	2.38	-0.53±2.7
A6NC20	Neutral alpha-glucosidase AB	GANAB			+			0.87±2.1		2.54±2.78		2.79±2.03	4.75	1.11±2.9
A6NDN2	Protein FAM3C	FAM3C		+	+	+		1.88±2.3		4.05±2.78	5.55	-2.6±2.32	2.97	-4.77±3.18 6.01
A6NEH4	Tetraspanin-3	TSPAN3			+	+		1.09±2.25		0.3±1.47		3.7±2.56	5.42	4.5±2.99 6.08
A6NGE3	Hemicentin-1	HMCN1		+				1.29±1.78		3.98±3.45	3.18	-0.28±1.82		-2.98±3.08
A6NH94	Matrilin-4	MATN4			+			0.87±1.59		-0.73±1.78		-2.01±1.99	2.42	-0.4±1.69
A6NHI3	Leukocyte immunoglobulin-like receptor subfamily A member 5	LILRA5				+		1.85±2.34		3.31±3.04		-2.05±2.62		-3.51±2.87 3.63
A6NJS5	Alpha-amylase 2B	AMY2B	+	+				2.59±2.11	3.79	2.57±2.17	3.37	-0.29±1.51		-0.27±1.83
A6NMP3	Mitochondrial enolase superfamily member 1	ENOSF1	+		+			2.54±1.94	4.17	0.24±1.72		-3.66±2.43	6.11	-1.36±1.77
A6NMR0	Peptidyl-glycine alpha-amidating monooxygenase	PAM	+	+				2.86±2.59	3.01	3.7±2.93	3.89	-0.33±1.57		-1.18±2.71
A6XMW0	Bone marrow proteoglycan	PRG2	+		+			4.27±2.78	6.17	0.14±1.17		-4.18±2.7	6.64	-0.05±1.37
A7VJG6	Galectin-9	LGALS9		+				1.91±2.78		4.27±3.05	5.01	1.21±2.27		-1.15±2.59

Supplemental material is neither peer-reviewed nor thoroughly edited by CJASN. The authors alone are responsible for the accuracy and presentation of the material.

A8K981	Dermatopontin	DPT	+				2.03±1.89	2.33	0.05±1.33		-2.76±2.29	3.47	-0.78±1.34	
A8KA14	Beta-galactoside alpha-2,6-sialyltransferase 1	ST6GAL1	+	+			5.29±3.35	7.16	4.68±2.78	8.76	-1.24±1.82		-0.62±1.77	
A8KA65	Rabankyrin-5	ANKFY1		+	+		1.7±1.84		4.2±3.3	3.94	3.01±2.84	2.67	0.51±1.8	
A8KAJ1	Microfibril-associated glycoprotein 4	MFAP4			+		5.99±3.58		3.81±3.36	3.07	1.62±2.34		3.8±3.12	
A8MTF8	Protein FAM3B	FAM3B			+		0.1±2.45		-2.09±2.52		-3.42±2.43	5.09	-1.23±2.93	
A8MVI4	Collagen alpha-1	COL18A1			+	+	0.38±1.29		2.39±2.35	2.46	-0.8±1.33		-2.81±2.47	3.09
A8UHA1	Ectonucleotide pyrophosphatase/phosphodiesterase family member 2	ENPP2	+				3.01±2.75	2.97	1.14±3.26		-1±2.73		0.87±2.87	
B0YIW2	Apolipoprotein C-III	APOC3			+		0.41±1.23		-0.93±3.01		-3.94±2.98	4.33	-2.6±2.7	
B1AMP9	Extracellular sulfatase Sulf-2	SULF2			+		1.91±3.61		2.76±2.45		-4.91±3.39	5.43	-5.76±4.42	
B2R4G0	Stromal cell-derived factor 1	CXCL12	+		+	+	2.92±2.71	2.82	-0.57±1.09		-7.58±4.04	15.66	-4.09±3	4.64
B2R579	Apolipoprotein D	APOD			+	+	0.55±1.33		0.26±1.36		-2.64±1.73	6.38	-2.34±1.94	3.54
B2R5F2	Uteroglobin	SCGB1A1			+		2.12±2.72		-1.1±2.42		-2.94±2.92	2.42	0.28±2.61	
B2R5J9	Cystatin-C	CST3			+	+	0.58±1.46		2.49±2.98		-2.38±2.29	2.58	-4.29±3.21	4.46
B2R5L2	Alpha-1-acid glycoprotein 2	ORM2			+		0.57±2.74		-1.72±3.47		-3.77±3.21	3.31	-1.48±3.75	
B2R5W7	Tetraspanin-7	TSPAN7			+		-0.01±1.57		1.7±1.96		2.71±2.2	3.65	1±1.66	
B2R692	Rho-related GTP-binding protein RhoB	RHOB			+		-0.64±1.32		0.5±2.68		3.76±2.67	5.06	2.62±2.66	
B2R699	Ganglioside GM2 activator	GM2A			+		-0.26±2.15		0.45±2.34		-2.24±2.31	2.24	-2.95±2.94	
B2R6W6	Procollagen-lysine,2-oxoglutarate 5-dioxygenase 3	PLOD3			+	+	0.35±1.48		1.27±2.93		4.9±3.47	5.12	3.99±3.02	4.32
B2R710	Beta-1,4-galactosyltransferase 1	B4GALT1			+		0.66±1.07		2.82±2.62	2.76	0.69±1.26		-1.47±2.21	
B2R7H0	Secreted and transmembrane protein 1	SECTM1	+				1.7±1.43	3.33	1.9±2.39		-0.81±1.34		-1.01±2.18	
B2R7L5	Cell adhesion molecule 4	CADM4			+		2.08±2.64		1.73±2.71		-2.64±2.36	2.98	-2.29±3.13	
B2R8F7	Cartilage intermediate layer protein 1	CILP	+				3.13±2.43	4.22	1.95±2.35		-1.74±2.57		-0.57±1.42	
B2R9E1	Procollagen C-endopeptidase enhancer 1	PCOLCE			+	+	0.76±2.84		1.49±2.22		-3.02±2.99	2.43	-3.75±3.02	3.75
B2R9M3	Beta-2-glycoprotein 1	APOH			+	+	0.33±1.58		0.56±2.56		-2.34±2.52	2.07	-2.57±2.4	2.74

Supplemental material is neither peer-reviewed nor thoroughly edited by CJASN. The authors alone are responsible for the accuracy and presentation of the material.

B2RAY2	Hepatitis A virus cellular receptor 2	HAVCR2				+			2.54±3.01		1.2±2.82		-3.59±3.33	2.76		-2.24±2.95
B2RBB1	Choline transporter-like protein 2	SLC44A2				+			1.11±1.88		1.51±1.84		2.15±1.76	3.6		1.75±2.18
B2RBZ1	Charged multivesicular body protein 4c	CHMP4C				+			1.71±2.2		2.51±2.94		1.36±1.32	2.53		0.56±3.13
B2RC40	Cathepsin Z	CTSZ		+					2.1±1.96	2.62	2.2±2.43		-1.28±1.53			-1.38±2.47
B2RCB7	Vacuolar protein sorting-associated protein 4A	VPS4A				+	+		1.9±2.04		2.41±2.36	2.47	1.33±1.33	2.38		0.82±2.46
B2RDA1	Osteopontin	SPP1				+	+		-0.92±2.62		1.03±4.55		-3.9±4.06	2.21		-5.85±4.81
B2RDA1	Osteopontin	SPP1				+	+		1.34±2.13		2.99±2.49	3.46	1.74±1.77	2.33		0.09±2.36
B2RDD4	Protein CREG1	CREG1				+	+		-0.27±1.76		2.23±2.7		5.62±3.12	11.78		3.12±3.14
B2RDK2	Transmembrane protein 176B	TMEM176B					+		2.51±2.4		2.47±3.21		3.47±3.13	2.93		3.51±3.02
B2RNK7	Sortilin-related receptor	SORL1					+	+	0.68±3.09		2.53±2.54		-3.81±3.51	2.8		-5.66±3.76
B2RUU0	Fibrillin-1 [Cleaved into: Asprosin]	FBN1					+	+	2.1±2.45		2.5±3.13		2.29±2.43	2.14		1.89±3.04
B2RXK3	Serine/threonine-protein kinase ULK3	ULK3					+		2.14±1.99	2.67	2.17±2.2	2.33	-0.12±1.26			-0.15±2.22
B3KMF3	Group XV phospholipase A2	PLA2G15		+	+				-2.69±2.81		1.33±2.98		5.78±3.62	7.28		1.76±3.26
B3KMZ3	Transmembrane 7 superfamily member 3	TM7SF3					+		0.92±2.91		0.48±1.89		-2.77±2.99	2.07		-2.34±2.61
B3KNY4	Kinesin light chain 3	KLC3					+		2.67±2.06	4.15	2.76±2.44	3.06	-0.78±1.62			-0.87±2.02
B3KPB0	Sialate O-acetyltransferase	SIAE		+	+				2.56±2.13	3.61	2.29±2.15	2.7	-0.42±1.6			-0.15±1.86
B3KT11	Alpha-amylase 2B	AMY2B		+	+				2.56±2.13	3.61	2.29±2.15	2.7	-0.42±1.6			-0.15±1.86
B3KT11	Alpha-amylase 2B	AMY2B		+	+				0.67±1.36		1.16±1.83		-1.25±1.84			-1.75±1.59
B3KTR6	Matrix remodeling-associated protein 8	MXRA8					+	+	1.99±2.65		-0.29±1.31		-8.68±4.62	15.47		-6.4±4.06
B3KUZ0	Interleukin-18-binding protein	IL18BP					+	+	1.9±1.61		1.95±1.97	2.34	1.26±1.38			1.21±1.83
B3KVB2	Abscission/NoCut checkpoint regulator	ZFYVE19					+		-0.17±1.42		1.94±2.6		3.66±2.71	4.54		1.54±2.25
B3KWK6	Alpha-L-iduronidase	IDUA					+		2.11±2.43		1.99±2.17		1.67±1.69	2.34		1.79±2.63
B3KY69	Serine incorporator 1	SERINC1					+		-0.7±1.4		1.4±2.48		4.7±2.74	9.46		2.6±2.71
B3Y612	Toll-like receptor 2	TLR2					+		3.31±2.46	4.65	2.18±2.44		-1.4±2.55			-0.26±1.36
B4DDP7	Semaphorin-7A	SEMA7A		+												

Supplemental material is neither peer-reviewed nor thoroughly edited by CJASN. The authors alone are responsible for the accuracy and presentation of the material.

C9J8S2	Retinoic acid receptor responder protein 2	RARRES2	+	+		4.92±3.16	6.91	3.91±2.81	4.93	-0.86±1.92		0.14±1.99	
C9J8Z4	Immunoglobulin superfamily member 8	IGSF8			+	1.53±2.1		1.02±2.46		-2.61±2.49	2.61	-2.09±2.53	
C9JA99	Protocadherin alpha-7	PCDHA7		+		3.49±2.74		2.78±2.39	3.24	0.88±1.35		1.59±2.64	
C9JB49	Hyaluronidase-1	HYAL1		+		0.14±0.79		1.88±1.58	3.42	0.85±1.18		-0.89±1.08	
C9JLE3	Glypican-3	GPC3		+		1.22±2.28		3.35±3.05	2.87	0.14±1.59		-1.99±3.09	
C9JMY1	Insulin-like growth factor-binding protein 2	IGFBP2		+	+	0.67±2.87		3.03±2.62	3.2	-2.52±3.43		-4.88±2.91	8.7
C9JQ15	Vitellogenesis membrane outer layer protein 1 homolog	VMO1			+	1.27±1.48		1.69±2.65		-2.8±1.96	5.22	-3.22±2.97	2.79
D2DFB0	G-protein coupled receptor family C group 5 member B	GPRC5B			+	0.77±1.2		1.46±1.66		1.44±1.34	2.76	0.75±1.54	
D3DP70	Alpha-1,6-mannosylglycoprotein 6-beta-N-acetylglucosaminyltransferase A	MGAT5		+		3.72±2.52		3.73±2.9	4.04	1.65±2.25		1.64±1.94	
D3DQ14	Tetraspanin-1	TSPAN1			+	0.89±2.93		1.18±2.86		2.85±2.99	2.18	2.56±3.46	
D3DQ23	EF-hand calcium-binding domain-containing protein 14	EFCAB14			+	0.79±2.05		2.23±2.29		-3.09±2.48	3.77	-4.52±3.11	5.51
D3DQ23	EF-hand calcium-binding domain-containing protein 14	EFCAB14			+	-0.02±1.8		1.36±2.27		1.76±1.67	2.64	0.38±2.43	
D3DQ6	CD82 antigen	CD82			+	3.54±2.55	4.09	1.64±2.36		-2.08±2.88		-0.17±1.39	
D3DSD5	A disintegrin and metalloproteinase with thrombospondin motifs 1	ADAMTS1		+		2.75±2.5	2.95	1.42±2.5		-1.99±1.91	2.59	-0.66±2.72	
D3DUT6	Calsyntenin-3	CLSTN3			+	0.65±2.08		3.13±2.64	3.39	2.24±2.13	2.64	-0.25±2.3	
D3DW20	Leucine-rich repeat transmembrane protein FLRT3	FLRT3			+	1.47±2.01		2.35±2.15	2.87	-0.42±1.31		-1.31±2.3	
D3DW77	Chondroitin sulfate proteoglycan 4	CSPG4			+	2.2±2.03	2.85	2.11±2.21		-0.31±1.64		-0.22±1.98	
D3DX28	Reticulon-4 receptor	RTN4R		+		1.53±2.59		2.97±3	2.34	-2.13±2.55		-3.57±3.31	2.78
D6RAX3	Protocadherin-1	PCDH1		+	+	3.4±1.3	9.79	3.93±1.85	9.6	1.92±1.34	6.34	1.39±1.81	2.47
D6RBI0	Prominin-1	PROM1		+	+	1.64±3.36		3.5±3.83		-4.38±4.28	2.49	-6.24±4.32	5.42
D6RBK3	Transmembrane anterior posterior transformation protein 1 homolog	TAPT1			+	-0.47±1.88		0.9±2.14		4.26±2.66	7.32	2.89±2.75	2.63
D6W543	Solute carrier family 35 member F6	SLC35F6			+	0.36±1.53		4.98±3.16	6.98	4.87±3.09	6.98	0.25±1.56	
E5RG79	Zinc finger homeobox protein 3	ZFHX3		+	+	4.26±2.68		0.7±2.05		-0.31±1.49		3.25±2.66	3.6
E5RGD9	Elongin-C	TCEB1			+	0.46±1.35		1.99±1.85	2.78	1.19±1.54		-0.34±1.46	
E7ER45	Maltase-glucoamylase, intestinal [Includes: Maltase	MGAM		+									

Supplemental material is neither peer-reviewed nor thoroughly edited by CJASN. The authors alone are responsible for the accuracy and presentation of the material.

E7EU32	Mannosyl-oligosaccharide 1,2-alpha-mannosidase IA	MAN1A1	+	+		1.16±1.11	2.7	2.97±2.39	3.76	1.15±1.27		-0.65±1.76	
E9PC35	Low-density lipoprotein receptor-related protein 2	LRP2			+	0.79±0.97		1.5±1.68		1.56±1.56	2.39	0.85±1.17	
E9PCD7	Epididymis-specific alpha-mannosidase	MAN2B2	+			3.69±3.04	3.62	2.3±3.27		0.32±2.52		1.72±3.06	
E9PHK0	Tetranectin	CLEC3B			+	0.18±1.73		0.98±2.98		-2.39±2.18	2.86	-3.19±3.29	
E9PHS0	LanC-like protein 1	LANCL1		+		3.34±2.94		2.61±2.24	3.25	0.39±2.09		1.13±2.25	
E9PQN9	Interferon-induced transmembrane protein 2	IFITM2			+	-0.9±2.51		1.67±2		2.22±2.24	2.35	-0.34±2.35	
E9PRA7	N-acyl-aromatic-L-amino acid amidohydrolase	ACY3		+		0.81±1.76		3.73±2.71	4.75	1.55±2.15		-1.37±1.8	
E9PS44	Interferon-induced transmembrane protein 1	IFITM1			+	-0.78±2.95		2.37±2.6		2.81±2.7	2.57	-0.34±2.92	
F5GYS9	Tumor necrosis factor receptor superfamily member 19L	RELT			+	0.62±2.76		0.53±1.7		-4.15±3.1	4.46	-4.06±3.05	4.39
F5H6E2	Unconventional myosin-1c	MYO1C			+	0.08±1.39		1.99±3.19		3.03±2.71	2.99	1.12±2.55	
F5H6I0	Beta-2-microglobulin [Cleaved into: Beta-2-microglobulin form pl 5.3]	B2M			+	0.84±1.4		0.24±1.58		-1.94±1.93	2.41	-1.35±1.65	
F5H6I0	Beta-2-microglobulin [Cleaved into: Beta-2-microglobulin form pl 5.3]	B2M			+	0.84±1.4		0.24±1.58		-1.94±1.93	2.41	-1.35±1.65	
F6X2W2	Neuronal growth regulator 1	NEGR1			+	2.21±2.66		0.59±1.74		-3.87±2.87	4.54	-2.25±2.44	
F8VNT9	CD63 antigen	CD63			+	-0.16±1.04		0.84±1.29		1.63±1.24	4.22	0.63±1.34	
F8VPC7	Endoplasmic reticulum chaperone	HSP90B1			+	-0.75±1.88		1.82±2.84		3.11±2.47	3.86	0.54±2.66	
F8W7D1	C3 and PZP-like alpha-2-macroglobulin domain-containing protein 8	CPAMD8		+	+	0.26±1.14		2.74±2.78	2.32	3.21±2.4	4.43	0.73±2.01	
F8W922	Multivesicular body subunit 12B	MVB12B			+	0.87±1.85		1.44±2.58		2.36±2.47	2.19	1.78±2.34	
G3V1D7	Reticulon-4 receptor-like 2	RTN4RL2		+		2.94±2.91	2.52	2.5±3		-0.37±2		0.07±3.06	
G3V3X5	Latent-transforming growth factor beta-binding protein 2	LTBP2		+		3.45±2.43	5.42	2.53±2.53		-1.84±2.54		-0.92±1.42	
H0Y543	Mannosyl-oligosaccharide 1,2-alpha-mannosidase IB	MAN1A2		+		1.16±1.11	2.7	2.97±2.39	3.76	1.15±1.27		-0.65±1.76	
H0YBK2	Protocadherin Fat 2	FAT2			+	0.5±1.44		2.71±3.3		3.06±3.04	2.41	0.86±2.17	
H0YKB2	Furin	FURIN		+		5.04±3.04	8.69	2.49±3.08		-0.88±2.39		1.68±2.35	
I3L0S5	Lysosomal alpha-glucosidase	GAA			+	1.13±1.27		1.84±1.85	2.38	0.23±1.33		-0.48±1.44	
J3KRC4	5'	NT5C			+	0.94±1.81		2.86±2.73	2.61	0.15±1.21		-1.76±2.77	

Supplemental material is neither peer-reviewed nor thoroughly edited by CJASN. The authors alone are responsible for the accuracy and presentation of the material.

P19835	Bile salt-activated lipase	CEL					1.74±2.22		2.66±2.28	3.26		0.23±1.1				-0.69±2.5	
P21145	Myelin and lymphocyte protein	MAL			+		-0.39±1.35		4.63±3.17	5.57		5.13±3.3	6.71			0.12±1.53	
P22492	Histone H1.4	HIST1H1E				+	1.59±2.69		-1.71±2.13			-5.26±3.22	7.92			-1.96±2.84	
P26992	Ciliary neurotrophic factor receptor subunit alpha	CNTFR				+	0.74±2.4		4.84±3.19	6.22		-0.18±2.57				-4.29±2.78	6.55
P34096	Ribonuclease 4	RNASE4					0.49±2.16		-2.5±2.03			-4.08±2.52	7.65			-1.08±2.29	
P53990	IST1 homolog	IST1				+	0.97±2.36		3.8±3.56	2.71		1.93±2.16				-0.9±3.26	
P78369	Claudin-10	CLDN10					0.3±1.54		1.97±2.37			2.69±2.11	3.98			1.02±2.17	
Q02383	Semenogelin-2	SEMG2				+	-4.45±5.36		-8.3±6.17	4.51		0.93±3.21				4.78±6.22	1.48
Q02487	Desmocollin-2	DSC2		+		+	6.08±3.39	9.85	3.69±2.88	4		-1.39±2.21				1.01±1.85	
Q14314	Fibroleukin	FGL2				+	1.03±2.54		3.22±3.19	2.44		0.67±2.2				-1.52±3.05	
Q15828	Cystatin-M	CST6					0.76±3.4		-0.23±2.3			-4.24±3.63	3.27			-3.24±3.36	
Q15848	Adiponectin	ADIPOQ				+	4.54±2.71		3.54±3.05	3.24		1.2±2.05				2.2±2.36	
Q16661	Guanylate cyclase activator 2B [Cleaved into: Guanylate cyclase C-activating peptide 2	GUCA2B				+	3.17±2.35	3.63	0.02±1.46			-3.88±2.88	4.56			-0.73±1.42	
Q4QQG1	FRAS1-related extracellular matrix protein 2	FREM2				+	1.67±2.56		3.84±3.8	2.44		1.85±2.81				-0.33±3.04	
Q4VC04	ProSAAS	PCSK1N					2.47±2.8		1.83±2.91			-3.84±3.61	2.7			-3.2±2.66	
Q5SZ76	Sialin	SLC17A5					1.87±2.58		0.3±1.84			2.99±2.95	2.44			4.55±2.8	7.74
Q695G9	C-type lectin domain family 14 member A	CLEC14A					1.42±1.93		0.26±2.38			-3.23±2.56	3.89			-2.08±2.46	
Q6UXB8	Peptidase inhibitor 16	PI16					0.94±2.27		0.05±1.7			-2.24±2.41	2.08			-1.35±2.12	
Q7Z7M8	UDP-GlcNAc:betaGal beta-1,3-N-acetylglucosaminyltransferase 8	B3GNT8				+	0.26±1.14		3.2±2.41	4.39		2.41±2.05	3.31			-0.53±1.38	
Q8IYS5	Osteoclast-associated immunoglobulin-like receptor	OSCAR					0.41±2.03		2.65±3.06			-1.71±2.38				-3.96±3.26	3.55
Q8ND23		CARMIL3					-4.15±3.04	4.87	-1.32±2.27			-0.88±1.67				-3.72±3.2	3.24
Q96FA3	E3 ubiquitin-protein ligase pellino homolog 1	PELL1				+	2.02±2.81		0.35±1.55			-5.34±3.18	8.76			-3.68±3.13	
Q9BRK3	Matrix remodeling-associated protein 8	MXRA8					0.67±1.36		1.16±1.83			-1.25±1.84				-1.75±1.59	2.9
Q9BTR7	Leucine-rich repeat-containing protein 40	LRRC40				+	0.13±1.63		5.19±3.51	5.75		4.87±3.49	4.94			-0.19±1.38	

Supplemental material is neither peer-reviewed nor thoroughly edited by CJASN. The authors alone are responsible for the accuracy and presentation of the material.

Q9HCN6	Platelet glycoprotein VI	GP6			+		1.82±2.55	-1.33±2.05	-3.77±2.72	4.85	-0.61±2.36
Q9UJU2				+	+	1.11±2.84	4.56±3.22	5.15	-1.34±2.74	-4.79±3.39	5.12
Total		50	90	151	61						

Supplemental material is neither peer-reviewed nor thoroughly edited by CJASN. The authors alone are responsible for the accuracy and presentation of the material.

Supplemental Table 2. Relative Operating Characteristic curve analysis value of CD133 ELISA assay for the comparison of autosomal dominant polycystic kidney disease (ADPKD) vs medullary sponge kidney (MSK), ADPKD vs Healthy Controls and MSK vs Healthy Controls.

	ADPKD vs MSK	ADPKD vs Healthy Control	MSK vs Healthy Control
AUC	0.82	0.98	0.7
AUC (95%CI)	(0.67-0.97)	(0.94-1)	(0.51-0.89)
P-values	0.003	<0.0001	0.047
Cutoff (RU/ml)	> 0.9850	> 0.4250	> 0.3850
Sensitivity%	53.33	93.33	53.33
Sensitivity% (95% CI)	(26.59-78.73)	(68.05-99.83)	(26.59-78.73)
Specificity%	93.33	94.44	88.89
Specificity% (95% CI)	(68.05-99.83)	(72.71-99.86)	(65.29-98.62)
Likelihood ratio	8	16.8	4.8

Supplemental material is neither peer-reviewed nor thoroughly edited by CJASN. The authors alone are responsible for the accuracy and presentation of the material.

References for Supplemental materials

1. Davis S, Charles PD, He L, Mowlds P, Kessler BM, Fischer R. Expanding proteome coverage with charge ordered parallel ion analysis (CHOPIN) combined with broad specificity proteolysis. *J Proteome Res.* 2017; 16(3):1288-99
2. Cox J, Mann M. MaxQuant enables high peptide identification rates, individualized p.p.b.-range mass accuracies and proteome-wide protein quantification. *Nat Biotechnol.* 2008;26(12):1367-72
3. Mallol R, Rodríguez MA, Heras M, Vinaixa M, Plana N, Masana L, Morris GA, Correig X. Particle size measurement of lipoprotein fractions using diffusion-ordered NMR spectroscopy. *Anal Bioanal Chem.* 2012; 402(7):2407-15
4. Inglis HC, Danesh A, Shah A, Lacroix J, Spinella PC, Norris PJ. Techniques to improve detection and analysis of extracellular vesicles using flow cytometry. *Cytometry A.* 2015; 87(11):1052-63
5. Cossarizza A, Chang HD, Radbruch A, Akdis M, Andrä I, Annunziato F, et al., Guidelines for the use of flow cytometry and cell sorting in immunological studies. *Eur J Immunol.* 2017; 47(10):1584-1797
6. Langfelder P, Horvath S. WGCNA: an R package for weighted correlation network analysis. *BMC Bioinformatics.* 2008;9:559
7. Hughes G. Youden's Index and the Weight of Evidence Revisited. *Methods Inf Med.* 2015;54(6):576-7